Physicochem. Probl. Miner. Process., 56(6), 2020, 178-193

http://www.journalssystem.com/ppmp

Physicochemical Problems of Mineral Processing

ISSN 1643-1049

Received August 15, 2020; reviewed; accepted October 07, 2020

Alumina-silica-titania adsorbent for hazardous azo and phtalocyanine dyes removal from textile baths and wastewaters – the impact of ionic surfactants

Małgorzata Wiśniewska [1], Katarzyna Wrzesińska [2], Monika Wawrzkiewicz [2], Stanisław Chibowski [1], Teresa Urban [1], Olena Goncharuk [3], Vladimir M. Gun'ko [3]

[1] Maria Curie-Sklodowska University in Lublin, Faculty of Chemistry, Institute of Chemical Sciences, Department of Radiochemistry and Environmental Chemistry, M. Curie-Sklodowska Sq. 2, 20-031 Lublin, Poland

[2] Maria Curie-Sklodowska University in Lublin, Faculty of Chemistry, Institute of Chemical Sciences, Department of Inorganic Chemistry, M. Curie-Sklodowska Sq. 3, 20-031 Lublin, Poland

[3] National Academy of Science of Ukraine, O. O. Chuiko Institute of Surface Chemistry, 17 General Naumov Str., 03164 Kiev, Ukraine

Corresponding author: wisniewska@hektor.umcs.lublin.pl (Małgorzata Wiśniewska)

Abstract: Two aspects of interfacial phenomena were discussed in the manuscript. The first one concerns the adsorptive removal of two azo dyes such as C.I. Acid Yellow 219 (AY219) and C.I. Direct Yellow 142 (DY142) as well as the phtalocyanine C.I. Reactive Blue 21 (RB21) on the alumina-silica-titania oxide (4% wt. Al_2O_3 – 8% wt. SiO_2 – 88% wt. TiO_2; AST88) in the ionic surfactants presence. The second one deals with the determination of interaction mechanism in the dyes-AST88, dyes-surfactant-AST88 systems using the data obtained from the surface charge density and zeta potential studies. The sodium dodecyl sulphate (SDS) with anionic character and hexadecyltrimethylammonium bromide (CTAB) with cationic ones were used. The adsorption capacities of 205.2 mg/g for AY219, 36.5 mg/g for RB21 and 18 mg/g for DY142. The potentiometric titration and Doppler laser electrophoresis methods enable determination of sign and magnitude of charge located in both the surface and the slipping plane layers around the solid particles. The structure of electrical double layer was determined in the AST88 systems without as well as with dyes and with mixed dye + surfactant adsorbates.

Keywords: dyes sorption removal, mixed oxide, ionic surfactants, dye-surfactant complexes, electrokinetic parameters

1. Introduction

The dynamic development of the textile, pulp-paper, chemical, tanning and cosmetics industry, contributes directly to the pollution of surface waters. It is estimated that 700 000 tons of various dyes are produced annually (Crini, 2016; Majewska-Nowak, 1986) and after different technological operations they are released directly into water reservoirs. The largest amounts of dyes are generated by the textile industry which is approximately 100 t of sewage throughout the year. The dyes containing effluents are a potential threat to animals and humans. In addition, sewage negatively affects the penetration of light through water, photosynthesis reactions and the production of oxygen in water by underwater plants. Moreover, some dyes are carcinogenic and show mutagenic character. Therefore it is necessary not only to purify purification of polluted waters carefully but also to reduce spills containing organic and inorganic acids, heavy metal ions, dyes and surfactants (Crini, 2016; Majewska-Nowak, 1986; Solecka and Ledakowicz, 2005; Kyziol-Komosinska et al., 2011). The presence of even very low concentrations, such as 1 mg/dm^3 of dye, can give an intense colour of water which indicates, that it cannot be used by people (Zeng et al., 2019). High toxicity was found in the case of C.I. Basic Violet 1 (LC_{50} = 0.05 mg/ dm^3, LC – lethal concentration (the dose required to kill half the members of a tested population)) and C.I. Basic Yellow 37 (LC_{50} = 0.8 mg/dm^3). Heavy metal ions such as Co, Cu,

DOI: 0.37190/ppmp/128214

Ni, Zn can be released from metal complex dyes, at high concentrations they are toxic and pose risks to living organisms. Therefore, dyes containing sewage treatment, becomes extremely important and its aim is to avoid possible risks for the environmental (Wang et al., 2012). Conventional methods of sewage treatment do not result in complete removal of colour. It is important to develop more effective methods of sewage treatment which would allow to reduce the charge of discharged pollutants as well as the recovery of water. Difficulties in developing economic and simple methods are mainly related to constant changes in the technology of dyes production and the use of different colours in technological processes (Crini, 2016; Majewska-Nowak, 1986). In the case of pollution that cannot be avoided it is worth neutralizing them using highly effective technologies. They can be combined to create multi-stage treatment systems. In this way several times reduction of several times of the pollution charge in sewage is achieved. Obtaining such effects is facilitated by the adsorption processes that allow, reduction contaminants concentration and separation of dissolved substances in accordance with selective interactions. The adsorption process is the most common method of inorganic and organic pollutants removal. It is characterized by high efficiency, simplicity and low costs (Afkhami et al., 2010). In terms of dyes adsorption, mainly ion exchangers, active carbon and clay minerals were studied (Wołowicz and Hubicki, 2016; Wawrzkiewicz, 2014; Wawrzkiewicz et al., 2017; Vhahangwele et al., 2015). It was found, that some new adsorbents should be designed to improve the separation and performance coefficients. Recently oxide adsorbents, such as aluminum or zirconium oxide, titanium dioxide and silica which can be used separately or in a mixed form have become an interesting area of research (Anbia and Salehi, 2012; Mahapatra et al., 2013). Mixed oxides have better catalytic properties compared to the pure form of oxides. For example, silica-aluminum oxide was used in the were acid catalyzed reactions. It is relatively stronger than pure oxide components. Titanium oxide and silica are characterized by special properties. They are thermally stable and have a large surface area and porosity. They are used as carriers for catalysts, optical systems and photocatalysts (Pabon et al., 2004; Mikushina et al., 2008). Moreover, mixed oxides are characterized by the presence of hydroxyl groups and a specific surface structure. Amphoteric groups can separate or attach a proton depending on the pH value, creating a constant surface charge. Oxide adsorbents have defined points of zero charge at which the value of the charged hydroxyl groups is the same. This parameter is extremely important because it describes the adsorption affinity and surface properties of the oxide which was used (Kosmulski, 2016; Khan et al., 2004; Phan et al., 2000; Liu et al., 2016). In recent studies high efficiency of mixed oxides to remove dyes has been obtained. The mixed cobalt and nickel oxide with the composition $Co_{0.4}Ni_{0.4}O_{0.2}$ was used to remove Congo Red and Methyl Blue. The sorption efficiency was 70% and 20%, respectively (Chowdhury et al., 2010). Silica materials characterized by porous structure, chemical reactivity and mechanical stability can be used as sorbents to remove pollutions caused by dyes (Yagub et al., 2014). Silicon dioxide showed very high affinity for C.I. Acid Blue 25 compared to other contaminants (2,4-dichlorophenoxyacetic acid or p-nitrophenol). In the case of the sorbent composed of 61.1% SiO_2 and 22.6% Al_2O_3, the Malachite Green, Methylene Blue and Rhodamine B were used as adsorbates (Khan et al., 2004). Removal of dyes ranged from 67.4% to 97.2%. This indicates that the material is suitable for dyes removal (Khan et al., 2004; Phan et al., 2000).

The objective of the paper was to remove the azo and phtalocyanine dyes from aqueous solutions using nanosized alumina-silica-titania oxide. This paper describes the properties of AST88 as an adsorbent for azo and phtalocyanine dyes for the first time. In order to establish applicability of AST88 as efficient adsorbent for dyes removal the sorption capacities were determined based on the Langmuir, Freundlich and Temkin isotherm models. Interpretation of kinetic measurements using the simple equations including the pseudo-first and pseudo-second order as well as intraparticle diffusion ones was made. The influence of different types of surface active agents on the dye adsorption on the nanosized oxide was taken into account. Another task of the paper was to investigate the suspension stability making the surface charge density and zeta potential measurements.

2. Experimental

2.1. Materials

The mixed oxide is composed of 4% wt. Al_2O_3, 8% wt. SiO_2 and 88% wt. TiO_2 was used as an adsorbent in the experiments. It was prepared at the Institute of Surface Chemistry of National Academy of

Sciences of Ukraine in Kiev by the pyrogenic method. This technique of mixed oxides synthesis involves a high-temperature hydrolysis of the corresponding metal tetrachloride ($Me[OCH(CH_3)_2]_4$) in a hydrogen-oxygen flame at 1100-1400 °C. It allows to obtain three-component oxides with colloidal dispersion as well as characterized by the developed specific surface area and different contents of individual components (Gun'ko et al., 2007). After the preparation process it was calcined at 450 °C - roasting of the solid below its melting point to remove water from its crystal lattice. The previous studies showed that the following species are present on the surface of AST mixed oxide particles dispersed in an aqueous solution: ≡SiO(H)Al≡, ≡SiO(H)Ti≡, ≡AlO(H)Ti≡ and ≡AlO(H)Si≡ (Gun'ko et al., 2017).

The disazo acid dyes, called C.I. Acid Yellow 219 and C.I. Direct Yellow 142 (Sigma-Aldrich, Germany) and also phthalocyanine dye, i.e. C.I. Reactive Blue 21 (Sigma-Aldrich, Germany) are used in the studies. These dyes are applied in the textile industry. Acid dyes are mainly used to dye wool, not cotton fabrics. Direct dyes work best on textiles with high contents of cellulose, such as cotton. Reactive dyes are most commonly used in dyeing of cellulose like cotton or flax, but also wool is dye able with reactive dyes. Reactive dyeing is the most important method for the coloration of cellulosic fibres. The physicochemical properties of dyes are presented in Fig. 1.

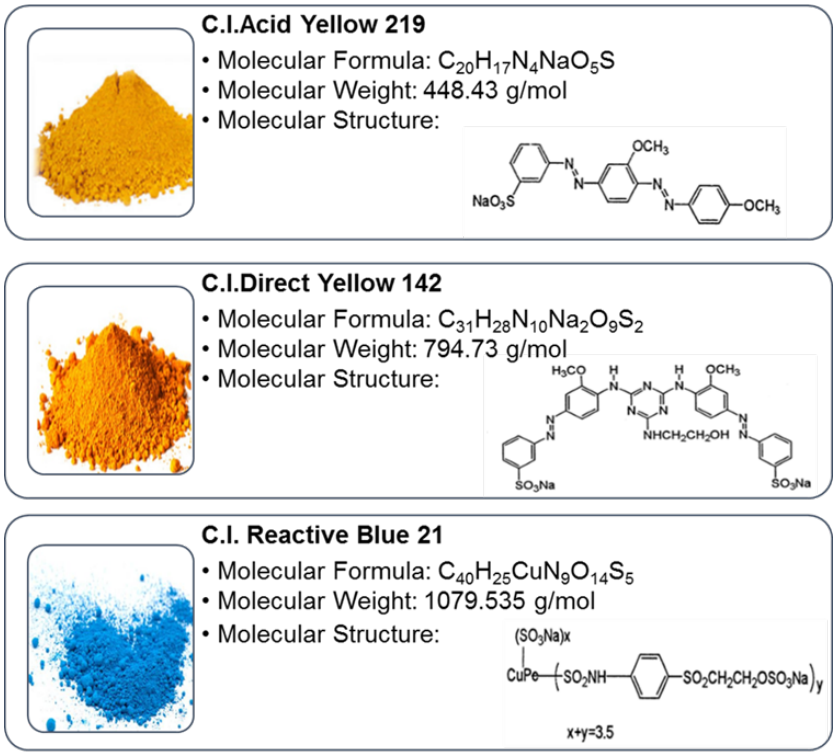

Fig. 1. Characteristics of C.I. Acid Yellow 219, C.I. Direct Yellow 142 and C.I. Reactive Blue 21

The surface active agents such as sodium dodecyl sulphate (SDS) and hexadecyltrimethylammonium bromide (CTAB) of laboratory grade were purchased from Sigma-Aldrich (Germany).

2.2. Methods

To analyze the textural characteristics of AST88 nanooxide, low-temperature (77.4 K) nitrogen adsorption–desorption isotherms were recorded using a Micromeritics ASAP 2405N adsorption analyzer. The samples were degassed at 110 °C for 2 h in a vacuum chamber. The values of the specific surface area (S_{BET}) were calculated according to the standard BET method (Gregg, 1982). The total pore volume V_p was evaluated by converting the volume of adsorbed nitrogen at p/p_0 = 0.98 – 0.99 (p and p_0 denote the equilibrium and saturation pressures of nitrogen at 77.4 K, respectively) to the volume of liquid nitrogen per gram of adsorbent. The nitrogen desorption data were used to compute the pore size distributions (PSD_S, differential $f_V \sim dV_p/dR$ and $f_S \sim dS/dR$) using a self-consistent regularization (SCR) procedure under non-negativity condition ($f_V \geq 0$ at any pore radius R) at a fixed regularization

parameter α = 0.01 with voids (V) between spherical nonporous nanoparticles packed in random aggregates (V/SCR model) (Gun'ko, 2014). The differential PSD_S with respect to pore volume $f_V \sim dV/dR$, $\int f_V dR \sim V_p$ were re-calculated to incremental PSD (IPSD) at $\Phi_V(R_i) = (f_V(R_{i+1}) + f_V(R_i))(R_{i+1} - R_i)/2$ at $\sum\Phi_V(R_i) = V_p$. The f_V and f_S functions were also used to calculate contributions of micropores (V_{micro} and S_{micro} at 0.35 nm < R < 1 nm), mesopores (V_{meso} and S_{meso} at 1 nm < R < 25 nm), and macropores (V_{macro} and S_{macro} at 25 nm < R < 100 nm).

Infrared diffuse reflection spectra with Fourier transform (IFF) of the samples were recorded using Fourier spectrometers Thermo Nicolet or Digilab Excalibur FTIR. To do this, a sample portion (4 mg) was mixed with KBr in a ratio of 1: 100, ground in a vibrating mill for 10 minutes. From the prepared mixture, a transparent plate with a size of 20x5 mm^2 was formed by pressing.

The diffraction patterns of the samples were recorded on the DRON-UM1 diffractometer in the radiation of the CoKα line of the anode with a graphite monochromator in the reflected beam at the geometry of the Bragg-Brentano image in the angle range of 10-80 degrees in step 0.05. They are digitally recorded in file: 2Θ (degrees) - Intensity. Phase identification was performed using a PDF-2 radiographic database (JCPDS Database, 2001). Silica was totally amorphous in all samples.

The X-ray photoelectron spectra (RFS) of the valence and internal levels of the AST88 sample were studied. The study was performed on the UHVAnalysis-System (SPECS, Germany). The system is equipped with a hemispherical analyzer PHOIBOS 150. During all experiments, the pressure of the ionization chamber of the system was less than $9 \cdot 10^{-8}$ Pa. Al Kα emitter (E = 1486.6 eV) was used as the causative agent of RFS radiation. RFS spectra were obtained at a constant control energy of 25 eV. The energy scale of the spectrometer was calibrated to the energy position of Au 4f7/2 and Cu 2p3/2, which are equal to 84.00 ± 0.05 eV and 932.66 ± 0.05 eV, respectively, relative to EF. The energy shifts due to charge effects were calibrated by RFS spectra of C 1s-electrons of hydrocarbons. The samples were placed on a molybdenum substrate.

The microcalorimetric investigations were carried out by means of a DAC1.1A (Chernogolovka, Russia) differential automatic calorimeter (Calvet and Prat, 1963). Differential automatic calorimeter was calibrated using known heat effect of dissolution of KCl in water (18.6 ± 0.012 kJ/mol at 20 °C). Before the measurements of the heat of immersion in water or n-decane, the samples (100 ± 2 mg) were degassed at 473 K and 0.01 Pa for 2 h and then used without contact with air. Glass ampoules with samples (100 ± 2 mg) were placed in the calorimeter cells with wetting liquid (3 cm^3) and thermostated at 298 K. Glass ampoules for immersion wetting studies have a special shape with thin curved tips of their end. For beginning measuring of immersion heat, the tips were broken by pressing and surrounding liquid permeated in vial and wetted the studied samples. Released heat of immersion was registered by differential calorimeter through the change of the temperature measured by thermopile detectors each composed of 960 thermocouples. The obtained results were recorded in the form of microcalorimetric curves with a typical peak (Goncharuk, 2015) integrated to calculate the thermal effects of immersion. The calorimeter was calibrated against the heat of dissolving of KCl. Since the total heat of immersion is dependent on the mass of sample under test and accordingly on its surface area, obtained results of measuring were normalized to 1 g of the sample and to 1 m^2 of its surface. For each sample, the measurement of heats of immersion in every liquid was performed 2–3 times and average value was calculated. The average errors of the Q measurements at multiple repeated measurements were 7%. To estimate the hydrophilicity of samples, the hydrophilicity indexes $K_h = Q_{water}/Q_{decane}$ were calculated (Rehbinder, 1979).

Adsorptive studies were carried out by the batch method. The experiments were performed out in flasks using a laboratory shaker Elphin 358S (Elpin+) with the constant speed and amplitude (180 cpm, 8 amplitude) at room temperature. 0.02 g of AST88 was shaken with 0.02 dm^3 of the dye solution of the known concentration from 1 to 240 min (kinetic studies) or 24 h (equilibrium studies). After the predetermined time interval AST88 was separated by the filtration. The dyes concentration in the aqueous phase was determined spectrophotometrically using a UV/Vis spectrophotometer Cary 60 (Agilent) at the maximum absorbance wavelength (387 nm for AY219, 400 nm for DY142 and 663 nm for RB21). The amounts of AY219, DY142 and RB21 uptake by AST88 was calculated at equilibrium (q_e) and at time t (q_t) using the following Eqs. (1-2):

$$q_e = \frac{(C_0 - C_e)}{m} \cdot V \quad (1)$$

$$q_t = \frac{(C_t - C_e)}{m} \cdot V \quad (2)$$

where: C_0, C_e and C_t [mg/dm^3] are the dyes concentrations in the solution before adsorption, at equilibrium and after sorption time t, respectively, V [dm^3] is the volume of the dye solution, and m [g] is the mass of ST20.

The analysis of the equilibrium results was made based on the following isotherm models: Langmuir, Freundlich and Temkin ones. The linear form of the equation of Langmuir isotherm is given as (Eq. 3):

$$\frac{C_e}{q_e} = \frac{1}{Q_0 b} + \frac{C_e}{Q_0} \quad (3)$$

where: C_e [mg/dm^3] is the concentration of dye in the equilibrium state, q_e [mg/g] is the quantity of dye adsorbed by the unit of the adsorbent mass in the equilibrium state, Q_0 [mg/dm^3] and b [dm^3/mg] are the constants of the Langmuir isotherms regarding the adsorption capacity and the absorption rate, respectively.

The Freundlich isotherm model has a linear form expressed by the formula:

$$\log q_e = \log k_F + \frac{1}{n} \log C_e \quad (4)$$

where: C_e [mg/dm^3] is the concentration of dye in the equilibrium state, q_e [mg/g] is the quantity of dye adsorbed by the unit of the adsorbent mass, k_F [mg/dm^3] and n are the Freundlich constants.

In the case of the Freundlich model an important parameter is the empirical constant n. If $n < 1$, the adsorption is of chemical nature whereas when $n > 1$ the adsorption is of physical nature. The Freundlich constants K_F and n, can be determined based on the intersection and slope of the graph log q_e vs log C_e.

The Temkin isotherm is expressed by the formula (Eq. 5):

$$q_e = \left(\frac{RT}{b_T}\right) \ln A + \left(\frac{RT}{b_T}\right) \ln C_e \quad (5)$$

where: b_T [J/mol] is the Temkin constant which is closely associated with heat of sorption, A [dm^3/g] is the constant of Temkin isotherm, R [8.31 J/mol K] is the gas constant, T [K] is the temperature [K].

The models used to describe the sorption kinetics of AY219, DY142 and RB21 on the mixed silica-alumina-titania oxide, namely the pseudo-first order Lagergren (PFO) and pseudo-second order Ho (PSO) are expressed in the following forms:

$$\log(q_e - q_t) = \log q_e - \frac{k_1}{2.303} t \quad (6)$$

$$\frac{t}{q_t} = \frac{1}{k_2 q_e^2} + \frac{1}{q_e} t \quad (7)$$

where: q_e and q_t [mg/g] are the quantities of the dye adsorbed at the equilibrium state and after the sorption time t, k_1 [1/min] is the adsorption rate constant determined from the pseudo-first order equation, k_2 [g/mg min] is the adsorption rate constant determined from the pseudo-second order equation.

In order to establish the influence of anionic and cationic surfactants on the dyes uptake by AST88 the dye solutions of the initial concentration 20 mg/dm^3 were prepared in the presence of 0.1 g/dm^3 of each of the mentioned surfactants. The phase contact time, AST88 mass and volume of dye solution were equal to 15 min, 0.02 g and 0.02 dm^3, respectively.

The electrokinetic measurements enable determination of the solid surface charge density σ_0 [μC/cm^2] and zeta potential ξ [mV] of mixed oxide particles from the following equations:

$$\sigma_0 = \frac{\Delta V c_b F}{mS} \quad (8)$$

$$U_e = \frac{2\varepsilon_0 \varepsilon \xi}{3\eta} f(\kappa a) \quad (9)$$

where: c_b [mol/dm^3] is the base (NaOH) concentration, F [C/mol] is the Faraday constant, m [g] is the solid mass in the suspension, S [m^2/g] is the specific surface area of the solid, ΔV [L] is the difference in the volume of base which must be added to bring the pH of suspension and reference solution to the specified value, U_e [cm^2/Vs] is electrophoretic mobility, ε is the dielectric constant, ε_0 [F/m] is the electric permeability of vacuum, η [Pa·s] is the viscosity, $f(\kappa a)$ is the Henry function.

This first parameter was obtained by the potentiometric titration (Janusz, 1994; Skwarek et al., 2014) carried out using a set consisting of: thermostated Teflon vessel, glass and calomel electrodes (Beckman

Instruments), PHM 240 pH-meter (Radiometer), laboratory stirrer, RE 204 thermostat (Lauda), automatic Dosimat 765 microburette (Metrohm) and computer with the "Titr_v3" software worked out by W. Janusz. The zeta potential was determined from the electrophoretic mobility measurements using the Zetasizer Nano-ZS (Malvern Instruments) equipped with the immersion dip cell. The pH of examined suspensions was determined using the pH-meter produced by Beckman Instruments, whereas they were sonicated using the Misonix XL-2020 device. The electrokinetic measurements were performed at the concentrations of dye 20 mg/dm^3 and surfactant 0.1 g/dm^3.

Potentiometric titrations were initiated by adding 0.05 dm^3 of appropriate solution into the Teflon vessel. Then HCl solution (with the concentration 0.1 mol/dm^3) was added to obtain the initial solution pH value of about 3.5. When equilibration was reached, the solution was titrated with NaOH solution (with the concentration 0.1 mol/dm^3). The analogous potentiometric titrations were performed in the systems containing mixed oxide, i.e. the AST/dye solution (or the mixed solution of the dye and surfactant). 0.3 g of the solid was used to prepare these suspensions.

The zeta potential of mixed oxide particles was determined from the elctrophoretic mobility data using the Henry's equation (Hunter, 1981; Ohshima, 1994). The samples were prepared adding 0.005 g of mixed oxide to 0.1 dm^3 of water or aqueous mixed (dye+surfactant) solution. After 2 minutes of sonication the suspension was divided into 8 parts. In each of them the appropriate pH value was determined, i.e. 3, 4, 5, 6, 7, 8, 9, 10 ± 0.1. The electrophoretic mobility of all samples was then successively measured.

3. Results and discussion

3.1. Mixed oxide characteristics

Fumed nanooxides are products of high-temperature synthesis, which causes the absence of pores in the primary particles (Table 1). The high temperature of synthesis of pyrogenic oxides causes a close morphology of nonporous primary nanoparticles regardless of their chemical structure, but in the process of synthesis the formation of secondary aggregates of particles, which leads to a secondary porous structure, which is a void in the packaging of primary particles. Incremental pore size distribution ($IPSD_V$) for AST88 is shown in Fig. 2. The $IPSD_V$ shows that the structure of the secondary aggregates of the sample AST88 shows mainly macroporosity according to the IUPAC classification. It should be noted that upon dispersing in an aqueous medium, the secondary structure is partially or completely destroyed by ultrasound or mechanical mixing, but the structure of the primary particles remains unchanged.

Table 1. Characteristic of sample of highly dispersed three-component nanocomposite SiO_2-·Al_2O_3-·TiO_2 (AST88)

C_{SiO_2} [wt.%]	C_{TiO_2} [wt.%]	$C_{Al_2O_3}$ [wt.%]	S_{BET} [m^2/g]	V_p [cm^3/g]
8	88	4	39	0.123

The IR spectra of surface OH groups on oxides with a hypersteichiometric environment of metal atoms (in alumina the coordination number (k.ch.) of Al atoms is 4-6, and k.ch. Ti in TiO_2 - 6) have a more complex structure because in addition to the terminal hydroxyls of the MOH, bridge MO(H)M with lower values of ν_{OH} are added. The presence of a larger set of surface OH groups (usually a higher concentration) on alumina, titanium dioxide and mixed oxides (Fig. 3), in comparison with silica, greatly changes the properties of adsorbed water. The appearance of several peaks at 3642-3648, 3663-3673, 3685-3690 and 3710-3715 cm^{-1} (AST88) can be explained by the fact that the corresponding groups ≡$M_1O(H)M_2$≡ with isomorphic substitution of M1 on M2 in the phase M1, M2 on M1 in the M2 phase and on the boundary of the two phases will have different frequencies in the IR range (Fig. 3), and therefore their acidity will also be different. It is possible that in this area there are also oscillations of water molecules in the vapor phase, which are not fully compensated.

The crystallinity of simple and complex mixed oxide depend on the crystallinity of titania or alumina since silica is always amorphous (Fig. 4). AST88 sample includes both anatase and rutile (Fig. 2): due to

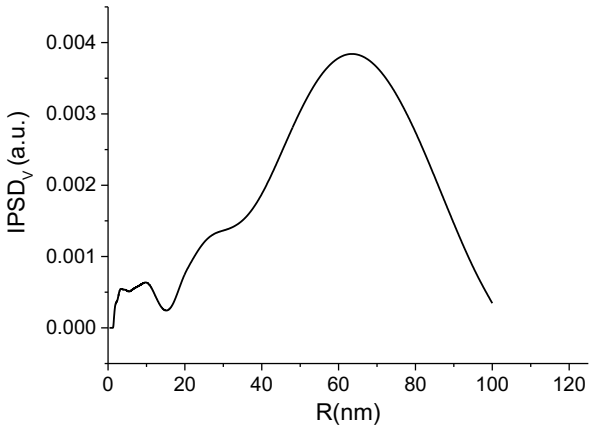

Fig.2. Incremental pore size distribution ($IPSD_V$) for fumed mixed oxide ACT88 (model of pores as voids between spherical particles)

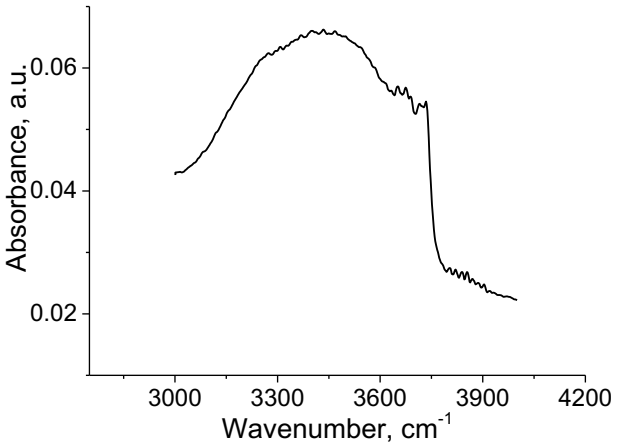

Fig. 3. FTIR spectrum of fumed oxide AST88 at 473 K in the region of valence vibrations of surface OH groups and adsorbed water

the high content of titanium dioxide, its crystal structure is closer to the individual fumed titanium disoxide, which also contains both phases - rutile and anatase, in contrast to other mixed ternary oxides, which are characterized by predominantly anatase. For other titania-containing fumed mixed oxides, titania is composed mainly of anatase (Gun'ko et al., 2016). This is of importance because the crystallinity degree and type of titania could influence the adsorption, catalytic, and other important characteristics of the materials.

Table 2 presents the elemental composition of near-surface layers of AST88 nanocomposite according to RFS spectra.

Fumed triple oxide AST88 demonstrates hydrophilic properties of the surface, which is appeared in a higher value of the heat of immersion in polar water (Q_w) than in non-polar n-decane (Q_d). Hydrophilicity index K_h=2.1, which is a prerequisite for good redispersing in the aqueous media (Table 3).

Table 2. Elemental composition of near-surface layers of AST88 nanocomposite

Total TiO_2 content [% wt.]	The ratio of atomic concentrations of oxygen and cations O/(Ti+Al+Si)	Surface concentration of elements [% at.]				
		Si (Si-O)	Al	Ti	O	Cl
88	1.62	5.3	4.8	27.7	61.5	0.7

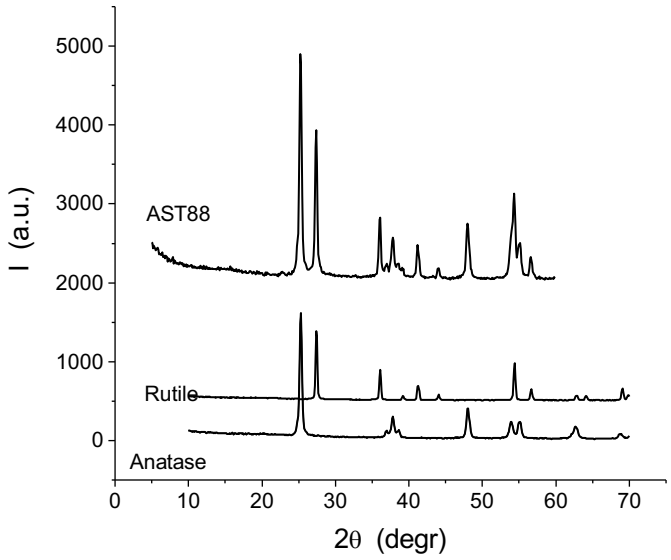

Fig. 4. XRD patterns of AST88 sample

Table 3. Heat of immersion of AST88 in water and n-decane

Q_w		Q_d		K_h
J/g	J/m²	J/g	J/m²	
24.8	0.63	11.81	0.30	2.1

3.2. Adsorption studies

The relation between the quantity of substance adsorbed at a constant temperature and its concentration in a solution in the equilibrium state is commonly called the adsorption isotherm. Parameters which were obtained from various models of isotherms, provide among others, information about surface properties of the adsorbent and also the sorption mechanism. In order to describe the above relations in the precisely AY219-AST 88, DY142-AST88 and RB21-AST88 systems, the most common isotherm models (Langmuir, Freundlich and Temkin) were applied.

In Table 4 the parameters of the above-mentioned isotherms are listed for AY219, DY142 and RB21 sorption from aqueous solutions on AST88. The maximum monolayer capacities Q_0 determined for the mixed oxide AST88 were equal to 205.2 mg/g, 36.54 mg/g and 18 mg/g for AY219, RB21 and DY142, respectively. The values of the correlation coefficients r^2 in the plot C_e/q_e vs C_e were equal to 0.989, 0.863, 0.985 for the dyes AY219, AY142 and RB21, respectively. Comparing the monolayer capacity values with the experimentally determined sorption values, it can be concluded that a satisfactory agreement of the experimental data and the Langmuir model was obtained as shown in Figure 5. Taking into account the type of the surface groups as well as porosity and surface of AST88, the monolayer formation is probable. Comparing the results with the literature data one can conclude about the efficiency of using mixed oxide to remove dyes from wastewater. Wawrzkiewicz et al. (2019) described the adsorption properties of the titania granulated adsorbent (known as Adsorbsia As 500) and found that the monolayer capacity was equal to 43.29 mg/g for RB21. The amounts of DY142 and AY219 retained by ST20 oxide (80% wt. SiO_2 and 20% wt. TiO_2) were 106.5 mg/g and 338.4 mg/g, respectively (Wawrzkiewicz et al., 2019; Wawrzkiewicz et al., 2019; Wiśniewska et al., 2018).

The correlation coefficients r^2 determining the appropriate fitting of the Freundlich and Temkin isotherms (Table 4) to the experimental data, based on the dependences log q_e vs log C_e and q_e vs ln C_e, were lower than for the Langmuir isotherm for AY219 and RB21, and slightly higher for DY142.

3.3. Kinetic studies

Analyzing Fig. 6 it can be stated the time necessary to reach equilibrium in the 20 mg/dm³ of dye (AY219, RB21, DY142) – AST88 system is very short. After 30 min of phase contact time the plateau is

Table 4. The values of isotherm parameters determined in the AY219-AST88, DY142-AST88 and RB21-AST88 systems

Dye	Parameters of isotherms								
	Langmuir			Freundlich			Temkin		
	r^2	Q_0 [mg/g]	b [dm³/mg]	r^2	k_F [mg/g]	n	r^2	A [dm³/g]	b [J/mol]
AY219	0.989	205.2	0.036	0.984	12.6	1.9	0.924	0.546	66.7
RB21	0.985	36.5	0.127	0.966	5.769	1.9	0.974	1.801	369.2
DY142	0.863	18.0	0.027	0.869	0.927	1.4	0.883	0.460	616.9

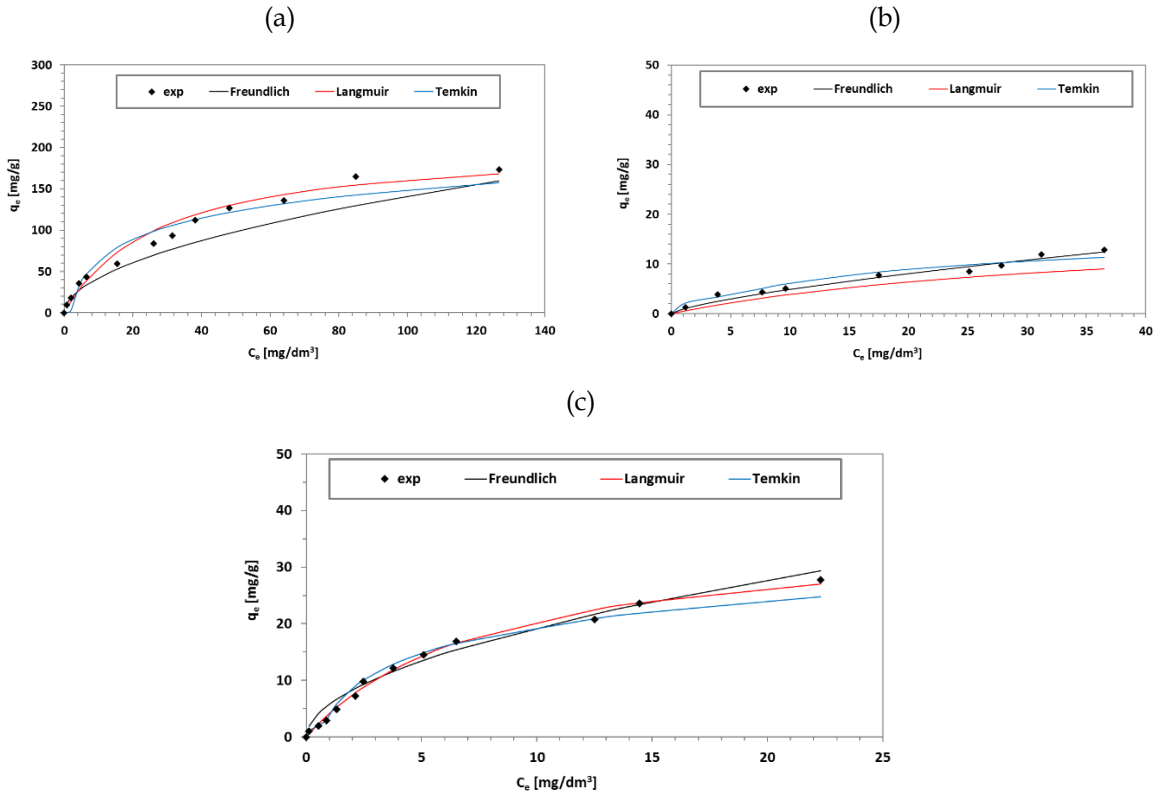

Fig. 5. Fitting of experimental data to three isotherms models in systems AY219-AST88 (a), DY142-AST88 (b) and RB21-AST88 (c)

observed. The amounts of dyes retained by AST88 in equilibrium were found to be 20 mg/g for AY219, 19 mg/g for RB21 and 18 mg/g for DY142 in the systems containing 20 mg/dm³ of dye before sorption. With the increase of the initial concentration of dye in the system (C_0=100 mg/dm³), it was observed that the time necessary to reach the state of equilibrium increased to 180 minutes. The q_e values were equal to 82.3 mg/g, 74.3 mg/g and 62.8 mg/g for AY219, RB21 and DY142, respectively (Table 5).

PFO and PSO models are based on the quantity of adsorbate determined by the unit of adsorbent mass relative to a specific time (q_t). The values of kinetic parameters determined from the respective graphs are presented in Table 5. A definitely better adjustment of experimental data was obtained for the pseudo-second order model (Fig. 6). This is evidenced by the obtained values of the correlation coefficients (r^2) and the calculated sorption capacities (q_e), which are close to the experimental data (q_{exp}). The dependence t/q_t vs t was linear over the entire concentration range of the dyes. It is believed that, the rate-limiting step is the surface adsorption involves chemisorption, where the removal from a solution is due to physicochemical interactions between the two phases. The pseudo-second order equation was widely applied for description of the experimental sorption data of dyes on different oxides such as titania, silica-titania and silica-alumina (Wawrzkiewicz et al., 2017; Wawrzkiewicz et al., 2019; Wawrzkiewicz et al., 2019).

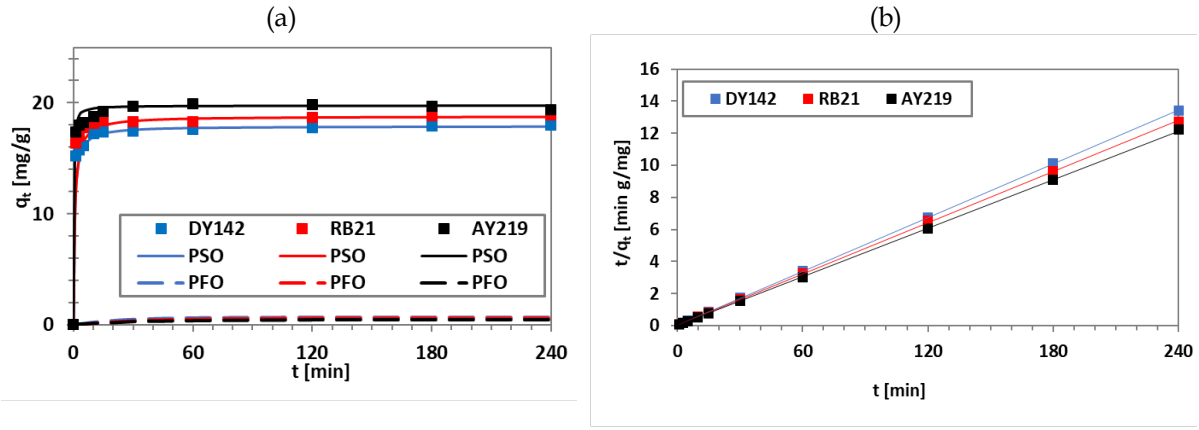

Fig. 6. Influence of phase contact time on the dyes adsorption from the 20 mg/dm³ systems and the fitting of experimental data to PFO and PSO kinetic models (a) as well as the PSO plot (b)

Table 5. Kinetic parameters of sorption in the AY219-AST88, DY142-AST88 and RB21-AST88 systems determined from the PFO and PSO models

Kinetic parameters	Initial concentration of dye C_0 [mg/dm³]					
	AY219		RB21		DY142	
	20	100	20	100	20	100
$q_{e,exp}$ [mg/g]	20	82.3	19	74.3	18	62.8
PFO						
q_e [mg/g]	1.1	40.2	1.4	26.3	1.5	22.2
k_1 [1/min]	0.011	0.035	0.013	0.016	0.018	0.018
r^2	0.426	0.971	0.811	0.935	0.706	0.897
PSO						
q_e [mg/g]	19.8	83.9	18.8	72.6	17.9	60.8
k_2 [mg/g min]	0.3796	0.0031	0.0779	0.0037	0.099	0.0039
r^2	0.999	0.999	0.999	0.998	0.999	0.995

Important step of the experiments was to establish the influence of surfactant addition on the dye retention by AST88. The dyeing baths and textile effluents contain different types of surfactants. It is worth to establish their impact on the dyes adsorption by different adsorbents as these auxiliaries can not only to increase the dye retention but also dramatically decrease the uptake. The effect of SDS and CTAB presence in the amount of 0.1 g/dm³ (below CMC of each surfactant) on the AY219, RB21 and DY142 sorption on AST88 from the solutions of the initial dye concentration 20 mg/dm³ was investigated and is presented in Fig. 7.

The drop in the amounts of the AY219, RB21 and DY142 adsorbed by AST88 was observed in the 20 mg/dm³ of dye – 0.1 g/dm³ of surfactant (SDS and CTAB) systems. In the case of anionic surfactant SDS, the observed drop of q_t can be explained by the competitive sorption of SDS anions in comparison with the anionic form of the dyes. Such an observation was described previously during C.I. Direct Blue 71 and C.I. Reactive Black 5 adsorption on the mixed silica-alumina oxide SA3 (97 wt. % SiO_2 and 3 wt. % Al_2O_3, (Wawrzkiewicz et al., 2017). In the case of cationic surfactant CTAB reduction of the amount of adsorbed dyes can be caused by the electrostatic interactions between the anionic form of the dye and the surfactant endowed with a positive charge.

3.4. Effect of surfactant addition on the electrokinetic properties of mixed oxide suspension

The analysis of curves of the surface charge density (σ_0) of AST88 as a function of solution pH presented in Fig. 8 indicates that the point of zero charge (pzc) of the mixed oxide is located at the pH value of approx. 4.8. Such value of pH_{pzc} is a result of the dominant content of titania (88%) in the triple oxide structure (Kosmulski, 2001). The surface -OH groups are of amphoteric character, i.e. depending on the

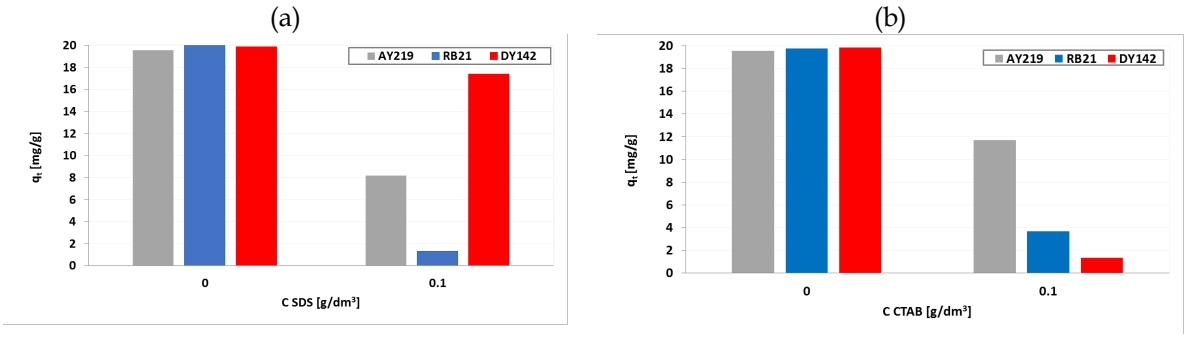

Fig. 7. Influence of surfactants addition: SDS (a), CTAB (b) on the dyes uptake by AST88

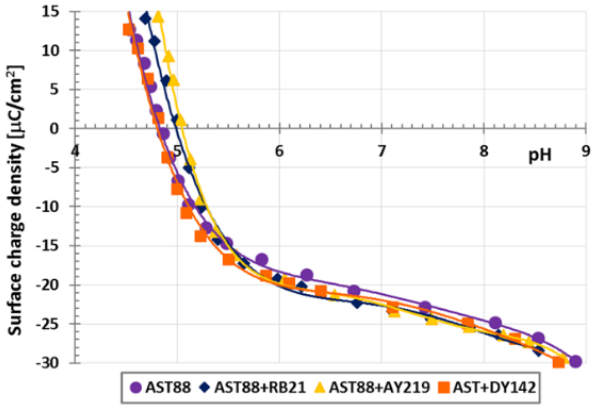

Fig. 8. AST88 surface charge density without and with adsorbed dye as a function of solution pH – influence of dye type

solution pH value they attach ($-OH_2^+$) or detach the proton ($-O^-$). Thus besides neutral hydroxyl groups, there are also positively and negatively charged groups on the mixed oxide surface. In the case of applied solid, the concentrations of positive and negative surface groups are the same at pH 4.8.

Regardless of the dye molecular weight, the structure of its molecule and the content of negatively charged sulphate groups, small changes in the surface properties of the solid in relation to the mixed oxide in the dye absence were observed. This may indicate the formation of hydrogen bonds between the azo moieties in the dye molecules and the AST88 surface hydroxyl groups. Such mechanism of adsorbate binding influences insignificantly both the solid surface charge density and location of pH_{pzc} points, and was observed in the other oxide systems (Wiśniewska, 2007; Wiśniewska, 2010). Formation of hydrogen bonds with the participation of ionized sulphate groups of the examined dyes is not excluded either but the scale of this phenomenon is rather marginal. The schematic representation of the binding mechanism through hydrogen bonds and electrostatic interactions is presented in Fig. 9.

The presence of ionic surfactants (anionic SDS and cationic CTAB) molecules in the adsorption layer has a significantly larger impact on the surface properties of AST dye systems (Fig. 10).

The presence of surfactant molecules in the AST88-AY219 system causes noticeable changes in the solid surface charge density (Fig. 10 (a)), but they are clearly smaller than those obtained for the AST88-RB21 (Fig. 10 (b)) and AST88-DY142 (Fig. 10 (c)) systems. The specific structure of the C.I. Acid Yellow 219, which is analogous to that of the surfactant molecule (it is possible to distinguish a longer hydrophilic part and hydrophilic sulphate end group), leads to the possibility of dye-surfactant hydrophobic interactions. In addition, in the case of CTAB the electrostatic attractions between the oppositely charged hydrophilic groups of the dye and surfactant take place. Thus dye-surfactant complexes are formed in the solution. Nevertheless, their specific arrangement in the adsorption layer does not have a significant effect on the sign and magnitude of the mixed oxide surface charge.

In turn, in the case of the suspensions containing C.I. Direct Yellow 142 (and also C.I. Reactive Blue 21), which are terminated by negatively charged sulphate groups on two sides, hydrophobic interactions with surfactant molecules play an insignificant role. In the presence of anionic SDS rather competitive adsorption between the dye and the surfactant molecules with the same ionic character

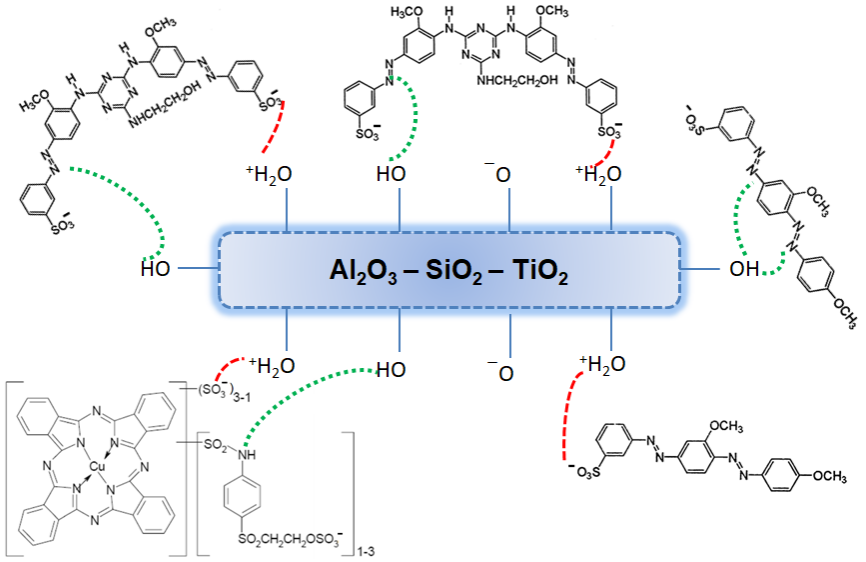

Fig. 9. The schematic representation of the binding mechanism of dye molecules through hydrogen bonds and electrostatic interactions on the AST88 surface

occurs whereas in the CTAB-containing system dye-surfactant complexes are formed (differently charged parts of molecules attract electrostatically).

Competitive adsorption of SDS and DY142 (or RB21) molecules results in an increase of the solid surface charge density in comparison to the system without the surfactant almost in the whole examined pH range, i.e. 5-9. Moreover, the anionic surfactant molecules are preferably bound with the AST surface groups - the negatively charged head of SDS interacts directly with the hydroxyl groups of mixed oxide causing the formation of an additional number of positively charged surface sites. On the other hand, the reduction of AST88 surface charge density in the systems containing both adsorbates indicates that the DY142-CTAB (or RB21-CTAB) complexes will rather remain in the solution and single molecules of cationic surfactant undergo adsorption on the mixed oxide surface. This leads to the creation of an additional number of surface sites endowed with a negative charge and reduction in the value of σ_0. Formation of another adsorption layer in which the surfactant molecules contact with the previously adsorbed layer with their hydrophobic parts is also possible.

The examined triple oxide is characterized by the isoelectric point (iep) equal to 7.6 (Fig. 11). At such pH value the zeta potential (ζ) is equal to 0 - the numbers of positive and negative charges accumulated in the slipping plane area are the same. For all used azo dyes, a significant reduction of zeta potential is observed in their presence within the whole studied pH range compared to the solid suspension without the dye.

As can be seen in Fig. 8 the greatest reduction of the electrokinetic potential of AST88 particles occurs in the presence of DY142 whereas the smallest in case of AY219. The reduction of the electrokinetic potential in these systems results mainly from the anionic nature of the dyes, as well as from their specific arrangement at the solid-solution interface which can lead to the shift of the slipping plane from the surface of the mixed oxide particles (Szewczuk-Karpisz et al., 2018; Szewczuk-Karpisz et al., 2019). The largest effect observed for by containing system DY142 indicates that the dye molecules were located in the adsorption layer in the way which exposes a large number of negative sulphate groups towards the bulk solution. This behaviour is very probable because the structure of DY142 is significantly expanded and ended on both sites with negatively charged sulphate groups. In addition, the adsorbed DY142 molecules do not pose such a large steric hindrance to other adsorbing dye molecules (in comparison to RB21) and a greater accumulation of negative charges in the area of the slipping plane is possible.

Figure 12 show the zeta potentials of AST88 particles dispersed in the systems containing mixed adsorbates - the dye and the surfactant. For all AST88-dye systems a significant increase in the electrokinetic potential in the presence of cationic CTAB was observed- in the whole examined pH range

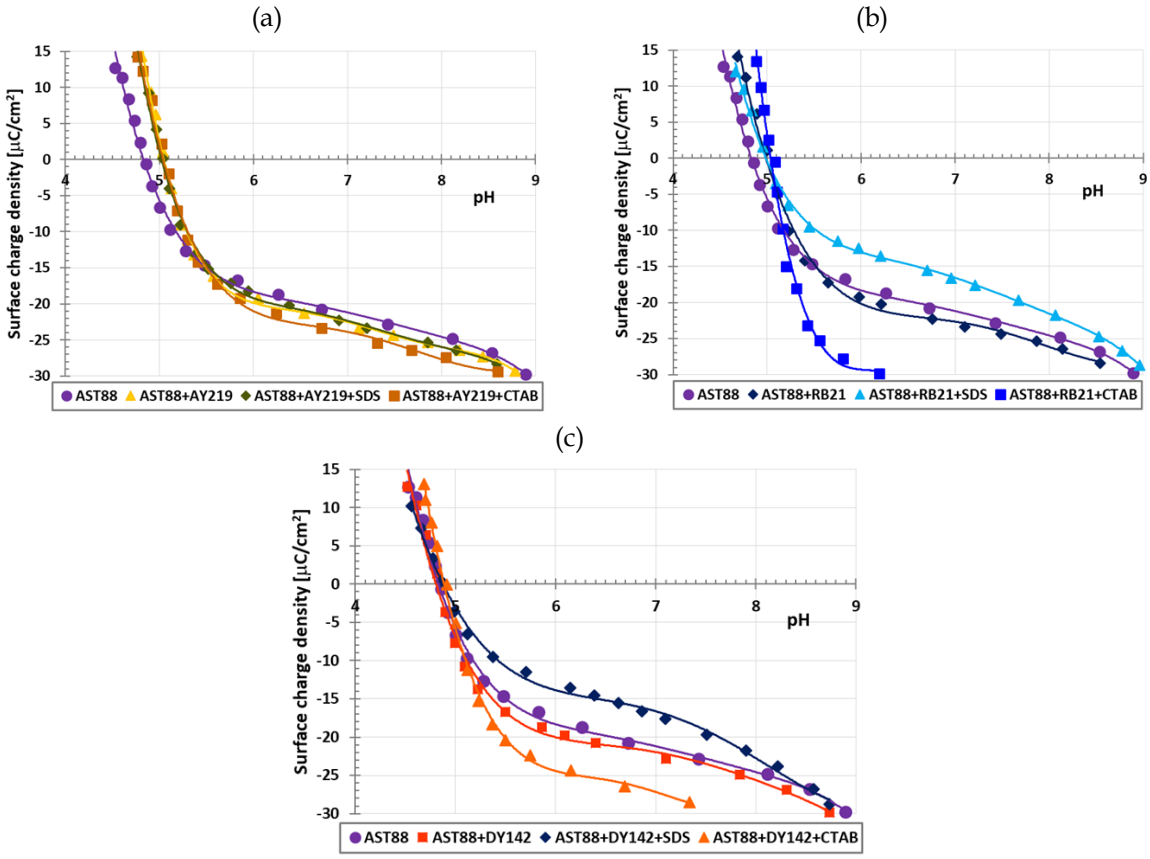

Fig. 10. AST88 surface charge density without and with adsorbed AY219 (a), RB21 (b) and DY142 (c) dye as a function of solution pH in the surfactant presence – influence of surfactant type

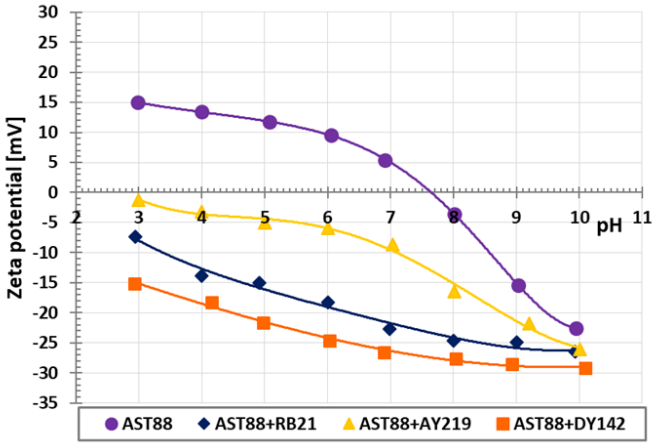

Fig. 11. AST88 particles zeta potential without and with adsorbed dyes as a function of solution pH – influence of dye type

ζ the potential assumes positive values from 20 to 30 mV. In turn, in the presence of anionic SDS the reduction of zeta potential is obtained compared to the system without surfactant.

The relatively high positive values of the electrokinetic potential confirm formation of the adsorption bilayer in the AST88-dye systems in the presence of cationic surfactant. The hydrophilic cationic CTAB heads located in the area of the slipping plane determine positive ζ potential of mixed oxide particles. On the other hand, the noticeable reduction of zeta potential of the AST88-dye systems containing anionic SDS is due to the specific structure of the adsorption layer composed primarily of dye-surfactant complexes (interacting with their hydrophobic fragments), but also individual molecules of both adsorbates, anionic parts of which are directed towards the liquid phase.

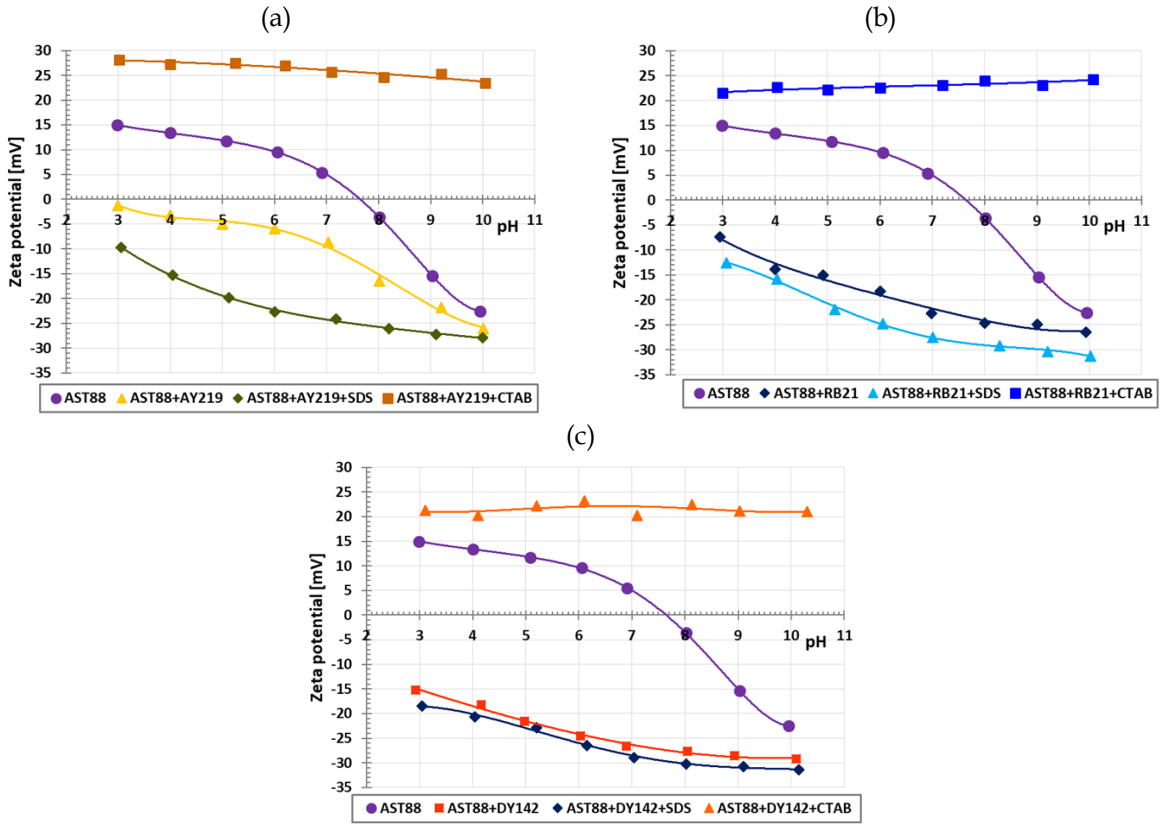

Fig. 12. AST88 particles zeta potential without and with adsorbed AY219 (a), RB21 (b) and DY142 (c) dye as a function of solution pH in the surfactant presence – influence of surfactant type

4. Conclusions

Adsorption studies revealed that the mixed oxide AST88 (4% wt. Al_2O_3 – 8% wt. SiO_2 – 88% wt. TiO_2) can be applied for azo and phtalocyanine dyes such as AY219, DY142 RB21 removal. Pseudo second order equation can be used for description of the kinetic sorption data in the systems containing 20 mg/dm^3 and 100 mg/dm^3 of dye. Based on the experimental equilibrium data and isotherm parameters calculated from the Langmuir model the highest affinity of AST88 for AY219 (205.2 mg/g) was obtained. Five times and eleven times less values of the sorption capacities were obtained in relation to RB21 and DY142, respectively. The anionic and cationic surfactant addition to the solution of the dye concentration 20 mg/dm^3 caused the decrease in the amount of dye uptake by AST88.

It was shown that the addition of azo dye affects the AST88 surface charge density slightly. This points to the formation of hydrogen bonds between the mixed oxide hydroxyl groups and the dye molecules. In turn, a distinct decrease of zeta potential of solid particles in their presence within the whole pH range compared to the solid suspension without the dye was observed. The presence of ionic surfactant molecules (SDS, CTAB) in the AST88-dye (AY219, RB21, DY142) systems causes considerable changes of the solid surface charge density in the case of RB21 and DY142 containing suspensions. Additionally, a significant increase in the electrokinetic potential of solid particles covered with dye adsorption layers in the presence of cationic CTAB and the reduction of this parameter in the presence of anionic SDS (compared to the system without the surfactant) were obtained. Thus, in the suspensions containing a mixture of both adsorbates dye-surfactant complexes were formed. They were characterized by various structures and different affinities for the triple oxide surface.

References

AFKHAMI, A., SABER-TEHRANI, M., BAGHERI, H., 2010. *Simultaneous removal of heavy-metal ions in wastewater samples using nano-alumina modified with 2,4 dinitrophenylhydrazine*. J. Hazard. Mater. 181, 836-844.

ANBIA, M., SALEHI, S., 2012. *Removal of acid dyes from aqueous media by adsorption onto amino-functionalized nanoporous silica SBA-3*. Dyes Pigments. 94, 1-9.

CALVET, E., PRAT. ,H., 1963. *Recent Progress in Microcalorimetry*, Pergamon.

CHOWDHURY, AL-N., RAHIM, A., FERDOSI, Y. J., AZAM, M. S., MUFAZZAL HOSSAIN, M., 2010. *Cobalt nickel mixed oxide surface: a promising adsorbent for the removal of PR dye from water*. Appl. Surf. Sci. 256, 3718-3724.

CRINI, G., 2016. *Non-conventional low-cost adsorbents for dye removal: a review*. Bioresource Technol. 97, 1061-1085.

GONCHARUK, O. V., 2015. *The heat of immersion of modified silica in polar and nonpolar liquids*. J. Therm. Anal. Calorim. 120, 1365–1373.

GREGG, S. J., SING, K. S. W., 1982. *Adsorption, Surface Area and Porosity*. Academic Press, London.

GUN'KO, V. M., 2014. *Composite materials: Textural characteristics*. Appl Surf Sci. 307, 444–454.

GUN'KO, V. M., NYCHIPORUK, Y. M., ZARKO V. I., et al, 2007. *Relationships between surface compositions and properties of surfaces of mixed fumed oxides*. Appl. Surf. Sci. 253, 3215–3230.

GUN'KO, V. M., TUROV, V. I., ZARKO, V. I., GONCHARUK, O. V., PAHKLOV, E. M., SKUBISZEWSKA-ZIĘBA, J., BLITZ, J. P., 2016. *Interfacial phenomena at a surface of individual and complex fumed nanooxides*. Adv. Colloid Interface Sci. 235, 108–189.

GUN'KO, V. M., PAKHLOV, E. M., SKUBISZEWSKA-ZIĘBA, J., BLITZ, J. P., 2017. *Infrared spectroscopy as a tool for textural and structural characterization of individual and complex fumed oxides*. Vibrat. Spectrosc. 88, 56-62.

HUNTER, R. J., 1981. *Zeta potential in colloid science*. Academic Press, New York.

JANUSZ, W., 1994. *Electrical double layer at the metal oxide/electrolyte interface in interfacial forces and fields: theory and applications*. In: M. Decker (Ed.), Surfactant Science, vol. 85, chapter 4, New York.

JCPDS Database, 2001. International Center for Diffraction Data, PA.

KHAN, T. A., SINGH, V. V., KUMAR, D., 2004. *Removal of some basic dyes from artificial textile wastewater by adsorption on Akash Kinari coa*l. J. Sci. Ind. Res. India. 63, 355-364.

KOSMULSKI, M., 2001. *Chemical properties of material surfaces*. Marcel Decker, New York.

KOSMULSKI, M., 2016. *Isoelectric points and points of zero charge of metal (hydr)oxides: 50 years after Parks' review*. Adv. Colloid Interfac. Sci. 238, 1-61.

KYZIOL-KOMOSINSKA, J., ROSIK-DULEWSKA, C., DZIENISZEWSKA, A., PAJAK, M., 2011. *Compost as biosorbent for removal of acid dyes from the wastewater generated by the textile industry.* Arch. Environ. Prot. 37, 3-14.

LIU, X. J., ZENG, H. Y., XU, S., CHEN, C. R., ZHANG, Z., DU, J. Z., 2016. *Metal oxides as dual-functional adsorbents/catalysts for Cu^{2+}/Cr(VI) adsorption and methyl orange oxidation catalysis*. J. Taiwan Inst. Chem. E. 60, 414-422.

MAHAPATRA, A., MISHRA, B. G., HOTA, G., 2013. *Adsorptive removal of Congo red dye from wastewater by mixed iron oxide–alumina nanocomposites*. Ceram. Int. 39, 5443-5451.

MAJEWSKA-NOWAK, K., 1986. *Usuwanie barwników ze ścieków przemysłowych*. Ochrona środowiska. 488/4, 17-22.

MIKUSHINA, Y. V., SHISHMAKOV, A. B., MATSKEVICH, V. V., ZHURAVLEV, N. A., KORYAKOVA, O. V., KHARCHUK, V. G., PETROV, L. A., 2008. *TiO_2-SiO_2 binary xerogels: synthesis and characterization*. Russ. J. Inorg. Chem+. 53. 1557-1560.

OHSHIMA, H., 1994. *A simple expression for Henry's function for the retardation effect in electrophoresis of spherical colloidal particles*. J. Colloid Interf. Sci. 168, 269-271.

PABON, E., RETUERT, J., QUIJADA, R., ZARATE, A., 2004. *TiO_2-SiO_2 mixed oxides prepared by a combined sol-gel and polimer inclusion method*. Micropor. Mesopor. Mat. 67, 195-203.

PHAN, T. N. T., BACQUET, M., MORCELLET, M., 2000. *Synthesis and characterization of silica gels functionalized with monochlorotriazinyl ß-cyclodextrin and their sorption capacities towards organic compounds*. J. Incl. Phenom. Macro. 38, 345-359.

REHBINDER., P. A., 1979. *Surface phenomena in disperse systems. Physicalchemical mechanics*. Moscow: Nauka Press (in Russian).

SKWAREK, E., JANUSZ, W., STERNIK, D., 2014. *Adsorption of citrate ions on hydroxyapatite synthetized by various methods*. J. Radioanal. Nucl. Chem. 299, 2027–2036.

SOLECKA, M., LEDAKOWICZ, S., 2005. *Biologiczne procesy oczyszczania barwnych ścieków włókienniczych*. Biotechnologia. 5, 103-124.

SZEWCZUK-KARPISZ, K., FIJAŁKOWSKA, G., SKIC, K., WIŚNIEWSKA, M., BOGUTA, P., KRASUCKA, P., SOKOŁOWSKA, Z., 2018. *Electrical double layer at the gibbsite/anionic polyacrylamide/supporting electrolyte interface – adsorption, spectroscopy and electrokinetic studies*. J. Molec. Liq. 261, 439-445.

SZEWCZUK-KARPISZ, K., KRASUCKA, P., BOGUTA, P., SKIC, K., SOKOŁOWSKA, Z., FIJAŁKOWSKA, G., WIŚNIEWSKA, M., 2019. *Anionic polyacrylamide efficiency in goethite removal from aqueous solutions*. Int. J. Env. Sci. Tech. 16, 3145-3154.

VHAHANGWELE, M., MUGERA, G. W., MUGERA, J., 2015. *The potential of ball-milled South African bentonite clay for attenuation of heavy metals from acidic wastewaters: simultaneous sorption of Co^{2+}, Cu^{2+}, Ni^{2+}, Pb^{2+}, and Zn^{2+} ions*. J. Environ. Chem. Eng. 3, 2416-2425.

WANG, X., GUO, Y., YANG, L., HAN, M., ZHAO, J., CHENG, X., 2012. *Nanomaterials as sorbents to remove heavy metal ions in wastewater treatment*. J. Environ. Anal. Toxicol. 2, 1000154.

WAWRZKIEWICZ, M., 2014. *Anion-exchange resins for C.I. Direct Blue 71 removal from aqueous solutions and wastewaters: effects of basicity and matrix composition and structure*. Ind. Eng. Chem. Res. 53, 11838-11849.

WAWRZKIEWICZ, M., POLSKA-ADACH, E., HUBICKI, Z., 2019. *Application of titania based adsorbent for removal of acid, reactive and direct dyes from textile effluents*. Adsorption. 25, 621-630.

WAWRZKIEWICZ, M., POLSKA-ADACH, E., WIŚNIEWSKA, M., FIJAŁKOWSKA, G., GONCHARUK, O., 2019. *Adsorptive removal of C.I. Direct Yellow 142 form textile baths using nanosized silica-titania oxide*. Eur. Phys. J. Plus. 134, 108-117.

WAWRZKIEWICZ, M., WIŚNIEWSKA, M., WOŁOWICZ, A., GUN'KO, V. M., ZARKO, V. I., 2017. *Mixed silica-alumina oxide as sorbent for dyes and metal ions removal from aqueous solutions and wastewaters*. Micropor. Mesopor. Mat. 250, 128-147.

WIŚNIEWSKA, M., 2007. *Temperature study of nonionic polymers adsorption at the alumina-solution interface*. J. Am. Ceram. Soc. 90, 3608-3614.

WIŚNIEWSKA, M., 2010. *Studies of temperature influence on adsorption behavior of nonionic polymers at the zirconia - solution interface*. J. Therm. Anal. Calorim. 101, 743-751.

WIŚNIEWSKA, M., WAWRZKIEWICZ, M., POLSKA-ADACH, E., FIJAŁKOWSKA, G., GONCHARUK, O., 2018. *Nanosized silica-titanium oxide as potential adsorbent for C.I. Acid Yellow 219 dye removal from textile baths and wastewater*. Appl. Nanosci. 8, 867-876.

WOŁOWICZ, A., HUBICKI, Z., 2016. *Carbon-based adsorber resin Lewatit AF 5 applicability in metal ion recovery.* Micropor. Mesopor. Mat. 224, 400-414.

YAGUB, M. T., SEN, T. K., AFROZE, A., ANG, H. M., 2014. *Dye and its removal from aqueous solution by adsorption: a review.* Adv. Colloid Interface Sci. 209, 172-184.

ZENG, M., WU, W., FANG, J., LI, S., ZHOU, Z., 2019. *Fabrication of chitosan/alginate porous sponges as adsorbents for the removal of acid dyes from aqueous solution*. J. Mater. Sci. 54, 9995-10008.